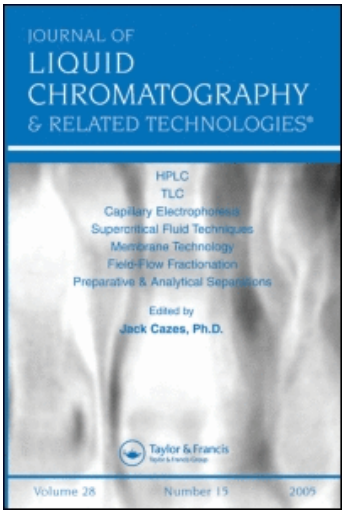

Journal of Liquid Chromatography & Related Technologies
Publication details, including instructions for authors and subscription information:
http://www.informaworld.com/smpp/title~content=t713597273

A NEW HYPOTHESIS ON THE HYDRODYNAMIC DISTRIBUTION OF THE UPPER AND LOWER PHASES IN CCC

Philip L. Wood[a]; Barry Jaber[a]; Ian A. Sutherland[a]
[a] Brunel Institute for Bioengineering, Brunel University, Uxbridge, UK

Online publication date: 30 June 2001

To cite this Article Wood, Philip L. , Jaber, Barry and Sutherland, Ian A.(2001) 'A NEW HYPOTHESIS ON THE HYDRODYNAMIC DISTRIBUTION OF THE UPPER AND LOWER PHASES IN CCC', Journal of Liquid Chromatography & Related Technologies, 24: 11, 1629 — 1654
To link to this Article: DOI: 10.1081/JLC-100104368
URL: http://dx.doi.org/10.1081/JLC-100104368

J. LIQ. CHROM. & REL. TECHNOL., 24(11&12), 1629–1654 (2001)

STUDIES OF LIQUID-LIQUID CIRCULATION

A NEW HYPOTHESIS ON THE HYDRODYNAMIC DISTRIBUTION OF THE UPPER AND LOWER PHASES IN CCC

Philip L. Wood,* Barry Jaber, and Ian A. Sutherland

Brunel Institute for Bioengineering, Brunel University,
Uxbridge, UB8 3PH, UK

ABSTRACT

This paper describes a theoretical explanation of why the lower phase always goes to the tail end of a coil when the tail is placed at the periphery. This effect is due to the Archimedean and Hydrostatic influences working together to pump the lower phase towards the tail and the upper towards the head. A combination of the planetary motion, the geometry of the helical coil, and the movement of the Interface between the phases generate the pumping effect.

INTRODUCTION

Traditionally, the head end of a coil has been defined as the end to which a bubble or bead would move under Archimedean rotation of the coil. The tail is the opposite end of the coil to the head. When the direction of rotation is reversed the head and tail ends of the coil are exchanged. Therefore, the position

*Corresponding author.

of the head or tail can be positioned to the requirements of the user. For example, in spiral wound coils, the head can be placed at the centre or periphery of the coil.

Hydrostatic pressures also play a role regarding spirally wound coils. If the Archimedean rotational movement were removed, the bead would move towards the periphery of the coil and the bubble would move towards the centre of the coil. Recent experimental research has shown that, for high β-values in a J-type centrifuge, the lower (more dense) phase will preferentially move towards the tail.[1] Under certain experimental conditions, the lower phase has moved towards the tail even when the tail has been placed at the centre of a coil. In this condition, the hydrostatic forces and Archimedean forces are working against each other. The best retention of stationary phase is obtained when the tail is placed at the periphery so that the Archimedean and hydrostatic influences are working together. In this configuration, experimental results showed that the upper phase was always driven towards the head, while the lower phase was always displaced towards the tail.[1]

These results were surprising, because the expected outcome was that the lower phase would be driven towards the head displacing the upper phase towards the tail. This paper puts forward a hypothesis on why the lower phase moves towards the tail, based on the following techniques:

Radial and tangential accelerations experienced by both phases, which are converted to Hydrostatic pressures.[2]

Newton's third law of motion.

The geometry of head-centre, tail-periphery coils.

The induced flow of each phase giving rise to piezometric pressures.

The pressure drop across the interface being equal to zero.

Numerical integration.

It is hoped that the explanation presented will help lead to a greater understanding of the pumping effects taking place in a J-type centrifuge.

THEORY

Let the pressure of both sides of the interface, at the distal key node, be P_d. Take a molecule of upper phase that is just radially inside the interface and a molecule of lower phase that is just radially outside the interface and place these molecules at the same angular position. As both of these molecules move away from the distal key node, the tangential component of hydrostatic pressure will decrease due to the tangential pressure gradient being negative. The tangential hydrostatic pressure will decrease more rapidly for the lower phase molecule than for the upper phase molecule, due to the greater density of the lower phase. There is now an imbalance across the interface. The upper phase has a greater hydrostatic pressure than the lower phase. This pressure imbalance will move the

interface radially outwards. This radial movement continues until the pumping effect of the interface movement creates a resisting pressure in the lower phase that equalizes the pressure imbalance and stops the movement of the interface.

The radial movement of the interface will also cause the radial component of hydrostatic pressure of the upper phase at the interface to change, and there will also be pressures induced in the upper phase due to the pumping effect of the interface. The radial component of hydrostatic pressure of the lower phase does not affect the pressure at the interface because radial hydrostatic pressure of the lower phase is always zero at the interface.

If the resultant pressure difference across the interface is assumed to be zero for all angular and radial positions of the interface, then the change in resultant pressure difference between any two points on the interface is also zero, hence:

$$\Delta P = 0 \tag{1}$$

Also:

Change in differential tangential hydrostatic pressure between the phases +
Change in radial hydrostatic pressure of upper phase +
Pressure difference due to local flow of the upper phase +
Pressure difference due to local flow of the lower phase = 0 (2)

In the steady state, the change in pressure will be equal on both sides of the interface for all radial and angular positions of the interface. The difference between the tangential pressures of each phase will cause the interface to move radially outwards as the distance from the distal key node increases. until the proximal key node is reached. Once passed the proximal key node, the interface will move radially inwards until the distal key node is reached.

From (2) the tangential and radial accelerations are:

$$\text{Tangential acceleration} = R\omega^2 \sin\theta \tag{3}$$

$$\text{Radial acceleration} = R\omega^2(\cos\theta + 4\beta) \tag{4}$$

However, these equations do not indicate the direction, in which the accelerations act; a free body diagram is required. Figure 1 is a free body diagram that was used to derive equations 5 and 6.

$$\text{Tangential acceleration} = R\omega^2 \sin\theta \tag{5}$$

$$\text{Radial acceleration} = -R\omega^2(\cos\theta + 4\beta) \tag{6}$$

The minus sign in front of equation 6 means that the direction of the acceleration is in the opposite direction to the arrow shown in figure 1 for the radial acceleration. Equations 5 and 6 represent the accelerations that the coiled tubing exerts upon the solvents. In order to calculate the hydrostatic pressures caused by

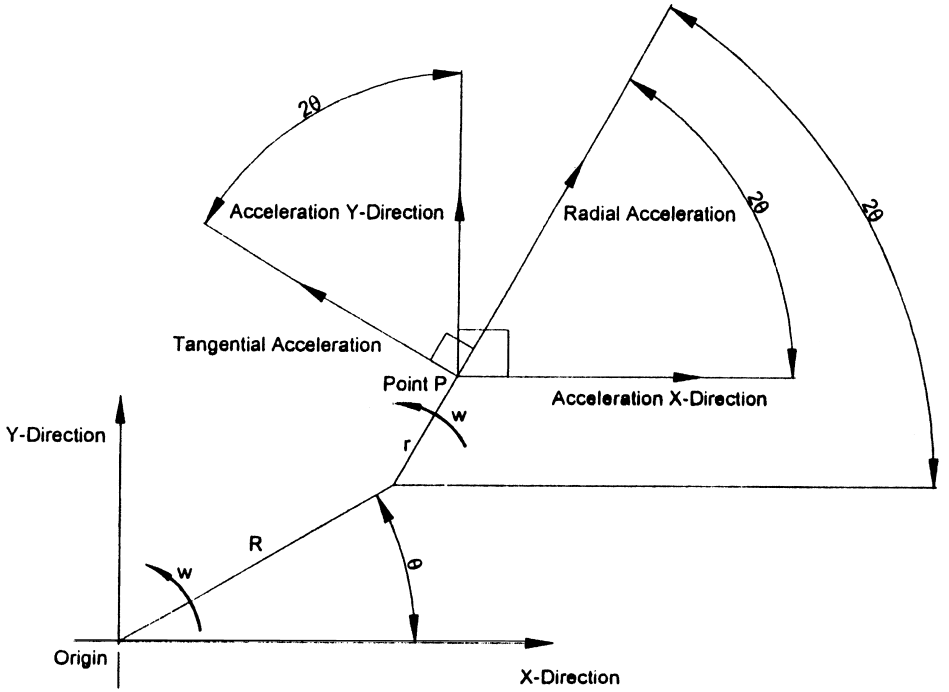

Figure 1. The free body diagram for resolving the x and y direction accelerations in the radial and tangential directions.

the tangential and radial accelerations, it is necessary to determine the accelerations that the solvents exert upon the coiled tubing. Newton's third law of motion states that if a particle P, that is part of the tubing wall, exerts an acceleration on a small volume of solvent adjacent to P then the small volume of solvent will exert an equal acceleration, but in the opposite direction. This means that equations 5 and 6 must be altered to indicate the change in direction in which the accelerations act, hence:

$$\text{Tangential acceleration} = -R\omega^2\sin\theta \tag{7}$$

$$\text{Radial acceleration} = R\omega^2(\cos\theta + 4\beta) \text{ since } \beta = \frac{r}{R} \text{ and}$$

$$\text{Radial acceleration} = \omega^2(R\cos\theta + 4r) \tag{8}$$

Equations 7 and 8 represent the accelerations that the solvents exert on the tubing. The minus sign in equation 7 shows that the Tangential acceleration is

acting in the opposite direction to the arrow shown in figure 1. The radial acceleration of the solvents is acting in the same direction as the arrow in figure 1. Equations 7 and 8, in the current form, can be used for deriving the hydrostatic pressures in helical wound coils.

Integration of the Change in Differential Tangential Hydrostatic Pressure

As the radius of the interface increases, the circumference length of the interface will also increase and, hence, the tangential pressure drop increases more than it would have done if the radius had remained constant. Therefore, the integration must be along the path of the interface, see figure 2:

$$dL_2 = (r_1 + dr)d\theta \text{ or } dL_2 = r_1 d\theta + dr d\theta \quad (9)$$

Multiplying equation 7 by the density of a phase will give the hydrostatic pressure gradient for that phase as follows:

$$\text{Tangential Hydrostatic Pressure Gradient} = -\rho R\omega^2 \sin\theta \quad (10)$$

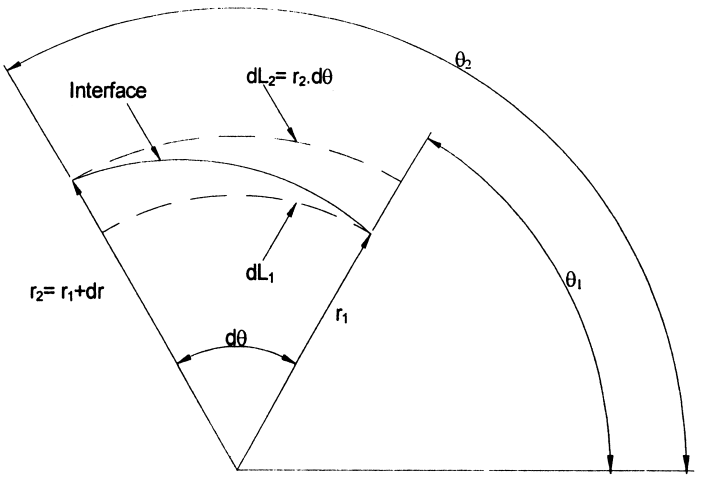

Figure 2. Basis of the formula for integration along the path of the interface in the tangential direction.

Therefore: $$\Delta P_{(Tangential)} = -\rho R\omega^2 \int_{L_1}^{L_2} \sin\theta dL_2 \quad (11)$$

Substituting equation 9 into equation 11 gives:

$$\Delta P_{(Tangential)} = -\rho R\omega^2 \int_{\theta_1}^{\theta_2} \sin\theta \left(r_1 d\theta + dr d\theta \right)$$

$$\Delta P_{(Tangential)} = -\rho R\omega^2 \left[\int_{\theta_1}^{\theta_2} \sin\theta r_1 d\theta + \int_{r_1}^{r_2} \int_{\theta_1}^{\theta_2} \sin\theta d\theta dr \right]$$

Integration and simplification leads to the following equation:

$$\Delta P_{(Tangential)} = -\rho R r_2 \omega^2 [\cos\theta_1 - \cos\theta_2] \quad (12)$$

Substituting the densities of the upper and lower phases into equation 12 permits the change in tangential hydrostatic pressure to be determined, see equations 13 and 14 below:

$$\Delta P_{(Tangential)Upper} = -\rho_U R r_2 \omega^2 [\cos\theta_1 - \cos\theta_2] \quad (13)$$

$$\Delta P_{(Tangential)Lower} = -\rho_L R r_2 \omega^2 [\cos\theta_1 - \cos\theta_2] \quad (14)$$

Equation 14 minus equation 13 gives the equation for the differential change of tangential hydrostatic pressure:

$$\Delta P_{Tangential} = -(\rho_L - \rho_U) R r_2 \omega^2 [\cos\theta_1 - \cos\theta_2] \quad (15)$$

Change in Radial Hydrostatic Pressure of the Upper Phase

Multiplying equation 8 by the density of a phase will give the hydrostatic pressure gradient for that phase as follows:

$$\text{Radial hydrostatic pressure gradient} = \rho\omega^2(R\cos\theta + 4r) \quad (16)$$

There is an exact solution for the change differential tangential hydrostatic pressure. The exact solution was possible because a relationship between dL_2, dr, and $d\theta$ could be derived. However, no such relationship can be derived for the radial hydrostatic pressure gradient, ie, no relationship between dr and $d\theta$ can be

derived because of the cosθ term in equation 15. The equation developed for the change in radial hydrostatic pressure will be inexact and will require a form of numerical integration to provide an accurate solution.

$\Delta P_{U(Radial)}$ = upper radial hydrostatic pressure at r_2, θ_2 - upper radial hydrostatic pressure at r_1, θ_1 providing that the angle between θ_2 and θ_1 is small.

$$\Delta P_{U(Radial)} = P_{2U(Radial)} - P_{1U(Radial)} \tag{17}$$

The radial Hydrostatic pressure at an angular position will depend upon the radial distance between the interface and the inner most radial surface of the tubing r_{in}.

$$P_{2U(Radial)} = \rho_U \omega^2 \int_{r_{in}}^{r_2} (R\cos\theta_2 + 4r)dr$$

$$P_{2U(Radial)} = \rho_U \omega^2 [Rr\cos\theta_2 + 2r^2]_{r_{in}}^{r_2}$$

$$P_{2U(Radial)} = \rho_U \omega^2 [Rr_2\cos\theta_2 + 2r_2^2 - Rr_{in}\cos\theta_2 - 2r_{in}^2] \tag{18}$$

By a similar process:

$$P_{1U(Radial)} = \rho_U \omega^2 [Rr_1\cos\theta_1 + 2r_1^2 - Rr_{in}\cos\theta_1 - 2r_{in}^2] \tag{19}$$

Substituting equations 18 and 19 into equation 17 gives:

$$\Delta P_{U(Radial)} = \rho_U \omega^2 [Rr_2\cos\theta_2 + 2r_2^2 - Rr_{in}\cos\theta_2 - Rr_1\cos\theta_1 - 2r_1^2 + Rr_{in}\cos\theta_1] \tag{20}$$

Piezometric Pressures Created Due to the Motion of the Interface

The movement of the interface causes a pumping action within the coil; the interface is acting in similar manner to the diaphragm in a diaphragm pump. This pumping action and, hence, the movement of the interface will be resisted by the viscosity of each phase. As there is no external pumping of either phase, the flow of each phase will depend upon the movement of the interface. As the tubing has a constant cross-sectional area, the flow of each phase will be equal but in opposite directions, hence:

$$Q_L = -Q_U = Q_{21} \tag{21}$$

Assuming that the flow of each phase is laminar the Hagen-Poiseuille equation can be used to determine the change in pressure between two adjacent positions using numerical integration:

$$Q_{21} = \frac{\pi r^4}{8\mu l}(P_2 - P_1) \qquad \text{(Hagen-Poiseuille)}$$

Rearranged, it becomes

$$\Delta P_{21} = (P_2\text{-}P_1) = \frac{8\mu l Q_{21}}{\pi r^4} \tag{22}$$

where
r = radius of tubing
μ = Dynamic viscosity
l = the length of tubing between positions 1 and 2
P_1 = the piezometric pressure at position 1
P_2 = the piezometric pressure at position 2
Q_{21} = the flow from position 2 to position 1 as $P_2 > P_1$

The differential tangential hydrostatic pressure decreases as distance from the distal key node increases, as stated above. The piezometric pressure in the lower phase must increase to help restore the pressure balance across the interface. Therefore:

$$\Delta P_{21L} = \frac{8\mu_L l_L Q_{21}}{\pi r_L^4} \tag{23}$$

Equation 21 showed that the flows of the upper and lower phases were equal but in opposite directions, therefore:

$$\Delta P_{21U} = \frac{-8\mu_U l_U Q_{21}}{\pi r_U^4} \tag{24}$$

The r_L and r_U are the equivalent radii of tubing that the phases would flow through depending upon the retention of each phase at each angular position. The values of these two variables will depend upon the position of the interface at a particular angular position.

Finding a Solution for the Radial Position of the Interface for Each Angular Position

Substituting equations 15, 20, 23, and 24 into equation 2 gives:

$$\rho_U \omega^2 [Rr_2 \cos\theta_2 + 2r_2^2 - Rr_{in} \cos\theta_2 - Rr_1 \cos\theta_1 - 2r_1^2 + Rr_{in} \cos\theta_1]$$
$$-(\rho_L - \rho_U) Rr_2 \omega^2 [\cos\theta_1 - \cos\theta_2] + \frac{8\mu_L l Q_{21}}{\pi r_L^4} - \frac{8\mu_U l Q_{21}}{\pi r_U^4} = 0 \tag{25}$$

The variables Q_2, r_L, and r_U must be derived in terms of r_1 and r_2. Once these variables are in terms of r_1 and r_2 the equation can be solved for r_1 or r_2.

The terms r_L and r_U represent the equivalent radii of tubing that the lower and upper phases would occupy in the coil tubing. The relationship between the coil tubing internal radius and the equivalent radii r_L and r_U is governed by the mean hydraulic depth (m) for circular tubes.

$$m = \frac{d}{4} = \frac{r}{2} = \frac{\text{Area}}{\text{Perimeter}} \tag{26}$$

$$r = \frac{2 \times \text{Area}}{\text{Perimeter}} \tag{27}$$

$$\therefore r_U = \frac{2 \times \text{Area of upper phase}}{\text{Perimeter of upper phase}} \tag{28}$$

$$\therefore r_L = \frac{2 \times \text{Area of lower phase}}{\text{Perimeter of lower phase}} \tag{29}$$

Area and Perimeter of a Circular Segment

For circular bore tubing, each phase will occupy a segment of the circular bore. This section derives the area equations and perimeter equations for the upper and lower phases. The area of a circular segment is the area of a circular sector minus the triangular area of the triangle with sides equal to r_t and third side equal to the cord length of the segment.

Area of a Circular Sector

$$\text{Area of Sector} = \frac{r_t e}{2}$$

where r_t = radius of tubing bore and e = arc length, see figure 3A

$e = \alpha r_t$

$$\therefore \text{ Area of Sector} = \frac{\alpha r_t^2}{2} \tag{30}$$

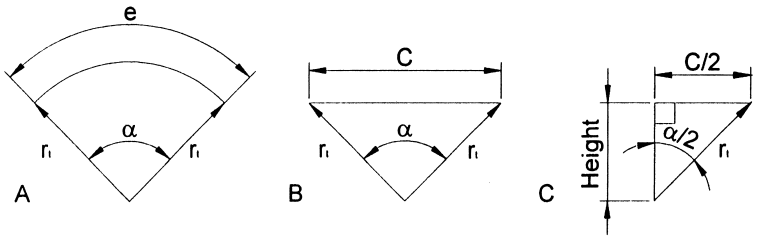

Figure 3. Sketches used to help derive the equations for the hydraulic mean depth.

Triangular Area

Area of a triangle is half the base length times the height. Let the cord length (c) of the segment be the base of the triangle, see figures 3B and 3C.

$$\therefore c = 2r_t \sin\left(\frac{\alpha}{2}\right) \tag{31}$$

$$\therefore \text{Height of the triangle} = r_t \cos\left(\frac{\alpha}{2}\right) \tag{32}$$

The area of a triangle is just: $r_t^2 \sin\left(\frac{\alpha}{2}\right)\cos\left(\frac{\alpha}{2}\right)$

Using the identity,

$\sin(2x) = 2\sin(x)\cos(x) \Rightarrow \frac{\sin(\alpha)}{2} = \sin\left(\frac{\alpha}{2}\right)\cos\left(\frac{\alpha}{2}\right)$ we get:

$$\text{Area of a triangle} = \frac{r_t^2 \sin(\alpha)}{2} \tag{33}$$

Area of a segment equals equation 30 minus equation 33:

$$\text{Area of segment} = \frac{r_t^2 (\alpha - \sin(\alpha))}{2} \tag{34}$$

Perimeter of Segment

The perimeter of the segment equals the cord length (c) plus the arc length (e).

$$\text{Perimeter of segment} = r_t\left(\alpha + 2\sin\left(\frac{\alpha}{2}\right)\right) \tag{35}$$

Mean Hydraulic Depth

Substituting equations 34 and 35 into equation 27 gives:

$$r = \frac{r_t\left(\alpha - \sin(\alpha)\right)}{\left(\alpha + 2\sin\left(\frac{\alpha}{2}\right)\right)} \tag{36}$$

For the upper phase let $\alpha = \alpha_U$

$$\therefore r_U = \frac{r_t\left(\alpha_U - \sin(\alpha_U)\right)}{\left(\alpha_U + 2\sin\left(\frac{\alpha_U}{2}\right)\right)} \tag{37}$$

For the Lower Phase substituting α_L for α in equation 34 gives:

$$\therefore \text{Area of lower segment} = \frac{r_t^2\left(\alpha_L - \sin(\alpha_L)\right)}{2}$$

Substituting $\alpha_L = 2\pi\text{-}\alpha_U$

$$\therefore \text{Area of lower segment} = \frac{r_t^2\left(2\pi - \alpha_U - \sin(2\pi - \alpha_U)\right)}{2}$$

Using the trigonometric identity sin(x-y) = sinxcosy-cosxsiny gives:

$$\therefore \text{Area of lower segment} = \frac{r_t^2\left(2\pi - \alpha_U + \sin(\alpha_U)\right)}{2}$$
$$\text{Perimeter of lower segment} = r_t\left(2\pi - \alpha_U + 2\sin\left(\frac{2\pi - \alpha_U}{2}\right)\right) \tag{38}$$

Again using the trigonometric identity sin(x-y) = sinxcosy-cosxsiny gives:

$$\therefore \text{Perimeter of lower segment} = r_t\left(2\pi - \alpha_U + 2\sin\left(\frac{\alpha_U}{2}\right)\right) \tag{39}$$

Substituting equations 38 and 39 into equation 27 gives:

$$\therefore r_L = \frac{r_t\left(2\pi - \alpha_U + \sin(\alpha_U)\right)}{\left(2\pi - \alpha_U + 2\sin\left(\frac{\alpha_U}{2}\right)\right)} \tag{40}$$

r_U and r_L are now in terms for α_U. The next task is to get α_U in terms of r_1 and r_2. Figure 4A and equation 31, modified for position 2, gives the height of the triangle as follows:

$$\text{Height of triangle} = r_t \cos\left(\frac{\alpha_{U2}}{2}\right) = r_t - h_2 \text{ and } h_2 = r_2 - r_{in}$$

$$\therefore \alpha_{U2} = 2\cos^{-1}\left(\frac{r_t - r_2 + r_{in}}{r_t}\right) \tag{41}$$

By a similar process, see figure 4B,

$$\alpha_{U1} = 2\cos^{-1}\left(\frac{r_t - r_1 + r_{in}}{r_t}\right) \tag{42}$$

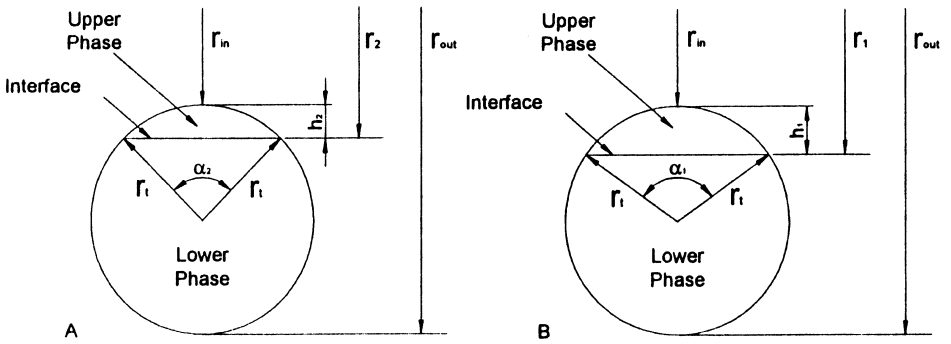

Figure 4. Sketches used to derive the equations for the radial position of the interface at positions 1 and 2.

Equation of Mean Flow in Terms of r_1 and r_2

Using: $Q_{21} = \frac{\Delta V}{\Delta t}$; $\omega\Delta t = \Delta\theta = \theta_2 - \theta_1$; $\therefore\ \Delta t = \frac{(\theta_2 - \theta_1)}{\omega}$, we form

$$\therefore\ Q_{21} = \frac{\Delta V \omega}{(\theta_2 - \theta_1)} \tag{43}$$

and $\Delta V = \Delta A l = (A_2 - A_1) l$

where l is taken as the mean length through which a phase flows between positions θ_2 and θ_1. Equation 25 cannot be solved for r_1 or r_2 without finding values for α_{U1} or α_{U2}. The values of α_{U1} or α_{U2} are used to determine the areas A_2, A_1 and, hence, the flow. As the solving routine within the software (MS Excel 2000) varies the value of r_1 or r_2, the new values of α_{U1} or α_{U2} have to be calculated, see equations 41 and 42. A similar solving routine is used to find the value of α_{U1} or α_{U2} corresponding to the value of r_1 or r_2 used. The software has not been written to allow for nested solving routines such as this and the software crashes. To overcome this shortcoming in the software, an approximation is used for ΔV.

The approximation used is (see figure 5):

$$\Delta V = \frac{(\text{Area of Sector to } r_2 - \text{Area of Sector to } r_1).c_2}{2}$$

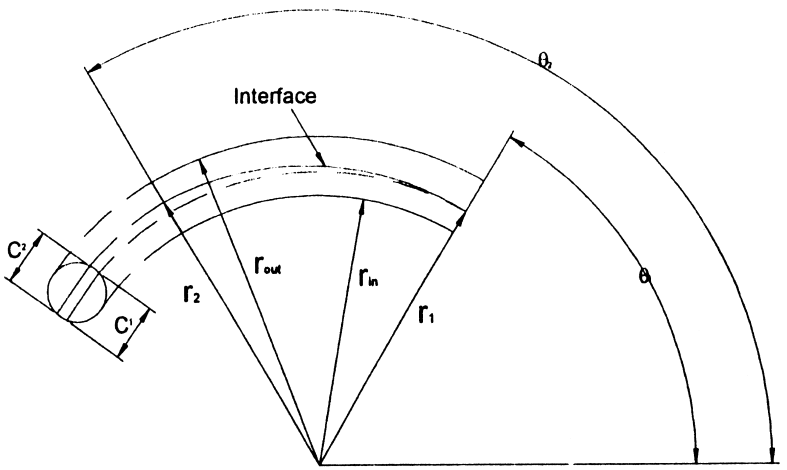

Figure 5. Sketch used to derive the equation for the change in volume of each phase between positions 1 and 2.

where c_2 is the cord length (equation 31) at position 2 and r_1 is the variable being solved for assuming that r_2 is already known and, hence, α_{U2} is also known.

$$c_2 = 2r_t \sin\left(\frac{\alpha_{U2}}{2}\right) \tag{44}$$

With the Area of Sector $= \frac{(\theta_2 - \theta_1)r^2}{2}$; $\therefore \Delta V = \frac{1}{2}\left(\frac{(\theta_2 - \theta_1)r_2^2}{2} - \frac{(\theta_2 - \theta_1)r_1^2}{2}\right)c_2$

is also equal to: $\frac{c_2(\theta_2 - \theta_1)\left(r_2^2 - r_1^2\right)}{4}$. Substituting in equation 43 for ΔV gives:

$$Q_{21} = \frac{c_2(\theta_2 - \theta_1)\left(r_2^2 - r_1^2\right)}{4}\frac{\omega}{(\theta_2 - \theta_1)} \text{ or}$$

$$\therefore Q_{21} = \frac{\omega c_2\left(r_2^2 - r_1^2\right)}{4} \tag{45}$$

Substituting equation 44 in equation 23 gives:

$$\Delta P_{21L} = \frac{8\mu_L l_L}{\pi r_L^4}\frac{\omega c_2\left(r_2^2 - r_1^2\right)}{4} = \left[\frac{\mu_L l_L}{r_L^4}\right]\left(\frac{2\omega c_2\left(r_2^2 - r_1^2\right)}{\pi}\right) \tag{46}$$

By a similar process:

$$\Delta P_{21U} = \left[\frac{\mu_U l_U}{r_U^4}\right]\left(\frac{-2\omega c_2\left(r_2^2 - r_1^2\right)}{\pi}\right) \tag{47}$$

The terms l_L, l_U, r_L and r_U in the square brackets are calculated in other columns. The equations 37 and 40 are used to calculate the values of terms r_U and r_L. The term l_L is the mean length that the lower phase flows along and is taken as the mean of r_1 and r_2 and then the combined mean of r_{out} and the mean of r_1 and r_2 times by the angular distance between θ_1 and θ_2. Hence:

$$l_L = \left(\frac{2r_{out} + r_1 + r_2}{4}\right)(\theta_2 - \theta_1) \tag{48}$$

By a similar process for l_U:

$$l_U = \left(\frac{2r_{in} + r_1 + r_2}{4}\right)(\theta_2 - \theta_1) \tag{49}$$

Finding a Solution for r_1 or r_2

Equation 25 is now replaced by substituting equations 15, 20, 45, and 46 in equation 2 to give:

$$\rho_U \omega^2 [Rr_2 \cos\theta_2 + 2r_2^2 - Rr_{in} \cos\theta_2 - Rr_1 \cos\theta_1 - 2r_1^2 + Rr_{in} \cos\theta_1]$$
$$-(\rho_L - \rho_U) Rr_2 \omega^2 (\cos\theta_1 - \cos\theta_2) + \left(\left[\frac{\mu_L l_L}{r_L^4}\right] - \left[\frac{\mu_U l_U}{r_U^4}\right]\right)\left(\frac{2\omega c_2}{\pi}\left(r_2^2 - r_1^2\right)\right) = 0 \tag{50}$$

Further substitutions for r_U from equation 37, r_L from equation 40, l_L from equation 47, and l_U from equation 48 can also be made, however, equation 49 will become very complex. The equation would become even more complex once equation 41 or 42 was substituted for the term α_{U1} or α_{U2} in equations 37 or 40 that are required to get the equation in terms of r_1 or r_2. Theoretically, this final equation could be solved algebraically, so that r_1 could be solved in terms of r_2 or visa versa. Once this equation was rearranged algebraically, it will have r^6, r^5 and r^4 terms. The equation will provide six solutions of which five will have to be rejected. The whole process of solving such a complex equation algebraically is extremely difficult for these reasons; the above equation has been solved numerically using the solving routine within Microsoft Excel.

Equations 37, 40, 41, 42, 45, and 46 were entered into an Excel spreadsheet. An initial radial position for the interface is selected for the Distal key node; the macros are then started and solutions are provided for the radial position of the interface for one complete loop of coiled tubing. Excel Macros were written that automated the use of the solving routine and takes the previous solution and uses it to help find the next solution. The angular step size used to obtain accurate numerical integrations in this manner was 0.25°.

RESULTS

The following parameters of a loop from a helical coil were entered into a spreadsheet using equation 49 and the supporting equations: β-value of 0.615, rotor radius (R) of 100mm and rotational speed of 800rpm. The β-value of 0.615 is the mean of the β-value range of the spiral coil used in Ref. [1].

For each phase system, listed in tables 1 and 2, a spreadsheet was run that had an initial condition for the interfacial distance of 1.5875mm at the distal key node. The final interfacial distance from this first spreadsheet was then used as the initial condition for a second spreadsheet. The retention of the upper phase was calculated for both the first and second spreadsheets. The volume of the loop under consideration was calculated. The change in retention of the upper phase between the first and second spreadsheets times by the loop volume, equals the change in volume of the upper phase. The first spreadsheet (figure 6) represents the position of the interface in the loop at time t and the second spreadsheet (figure 7) represents the position of the interface one revolution later, i.e., 0.075 seconds later at 800rpm. The change in volume of the upper phase divided by the 0.075 seconds gives the mean flow rate of each phase, since the loop has a constant volume. The flow of the lower phase is equal, but in the opposite direction to the flow of the upper phase. The results of this process are shown in table 3 and figures 6, 7, 8, 9, and 10. Figures 8 and 9 were produced by pasting the appropriate information from figures 6 and 7 and are intended to show the pumping effect in another manner to aid clarity.

Understanding figures 6, 7, 8, and 9:

1. The plotted curve shown is the position of the interface relative to the angular position in the coil.

Table 1. Chemical Composition of the Phase Systems and the Ratios of the Various Components

Phase System	Solvents	Ratios
2A	Heptane-Water	1:1
3A	Heptane-Isopropanol-Water	2.8:1.7:5.5
4A	Heptane-Ethyl Acetate-Methanol-Water	1.4:0.1:0.5:1
4E	Heptane-Ethyl Acetate-Methanol-Water	1.4:0.6:0.1:1
4B	Heptane-Ethyl Acetate-Methanol-Water	1.4:0.6:1:1
4G	Heptane-Ethyl Acetate-Methanol-Water	1.4:0.6:2:1
4D	Heptane-Ethyl Acetate-Methanol-Water	1.4:0.6:3.5:1
2C	n-Butanol-Water	1:1
4F	Heptane-Ethyl Acetate-Methanol-Water	1.4:2:1:1
4H	Heptane-Ethyl Acetate-Methanol-Water	1.4:3:1:1
2B	Ethyl Acetate-Water	1:1
3C	n-Butanol-Acetic Acid-Water	4:1:5
4C	Heptane-Ethyl Acetate-Methanol-Water	1.4:4.5:1:1
3B	Ethyl acetate-Acetic Acid-Water	4:1:4

Table 2. Physical Properties of the Phase Systems, 30ºC, Used for the Calculations, Values Taken From Ref. [9]

Phase System	Density kg/m^3	Density Difference kg/m^3	Dynamic Viscosity cp (mNs/m^2)	Interfacial Tension mN/m
2A Upper	658	336	0.36	
2A Lower	994		0.79	
3A Upper	674	290	0.38	
3A Lower	964		1.64	
4A Upper	679	268	0.36	17.8
4A Lower	947		1.36	
4E Upper	728	253	0.35	13.5
4E Lower	981		1.50	
4B Upper	708	230	0.35	6.2
4B Lower	938		1.35	
4G Upper	690	192	0.42	8.3
4G Lower	882		1.35	
4D Upper	683	169	0.35	5.5
4D Lower	852		1.01	
2C Upper	831	150	2.37	
2C Lower	981		1.02	
4F Upper	782	138	0.39	6.1
4F Lower	920		1.33	
4H Upper	814	114	0.41	1.2
4H Lower	928		1.34	
2B Upper	892	104	0.34	
2B Lower	996		0.93	
3C Upper	888	102	1.48	
3C Lower	990		1.32	
4C Upper	833	98	0.42	1.1
4C Lower	931		1.35	
3B Upper	926	79	0.68	
3B Lower	1005		1.15	

2. The upper phase is below the curve and the lower phase is above the curve. The phases are represented in this manner because the interfacial distance is measured from the radial innermost surface of the tubing.

3. The left and right-hand ends of the graph are distal key nodes and represent the start and finish of the loop under consideration. The position mid-way between the left and right end of the graph is the proximal key node.

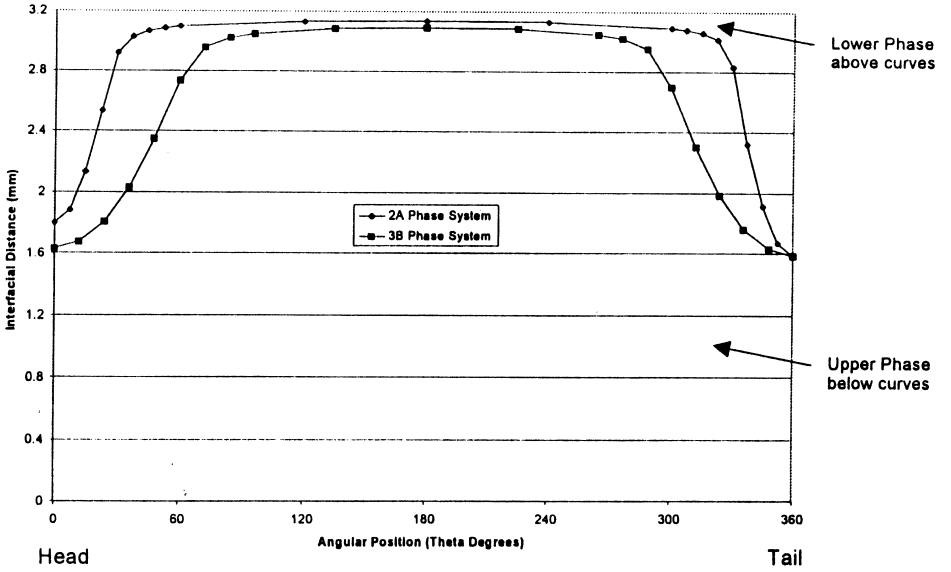

Figure 6. Positions of the interfaces for the 2A and 3B phase systems for the 1st calculation mode (see text). The interfacial positions for all other phase systems lie between these two curves.

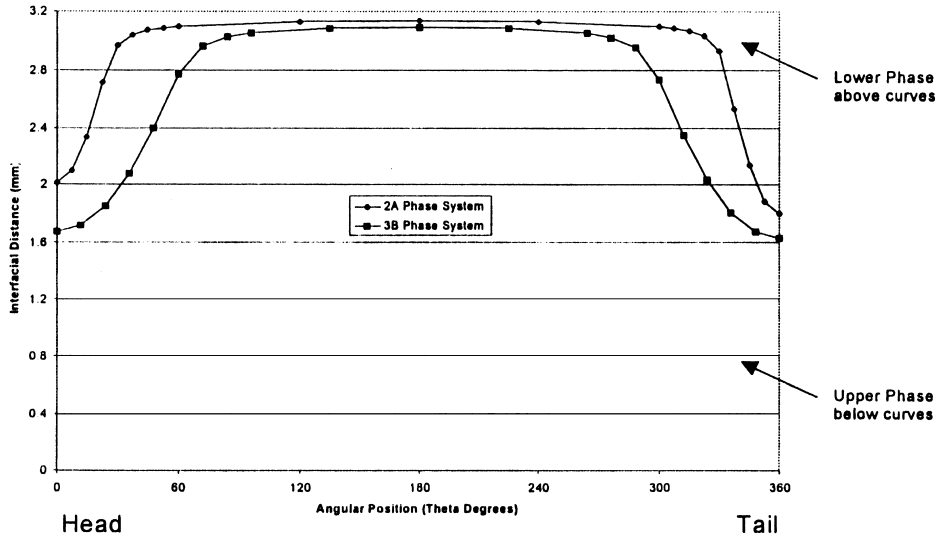

Figure 7. Positions of the interfaces for the 2A and 3B phase systems for the 2nd spreadsheet. The interfacial positions for all other phase systems lie between these two curves.

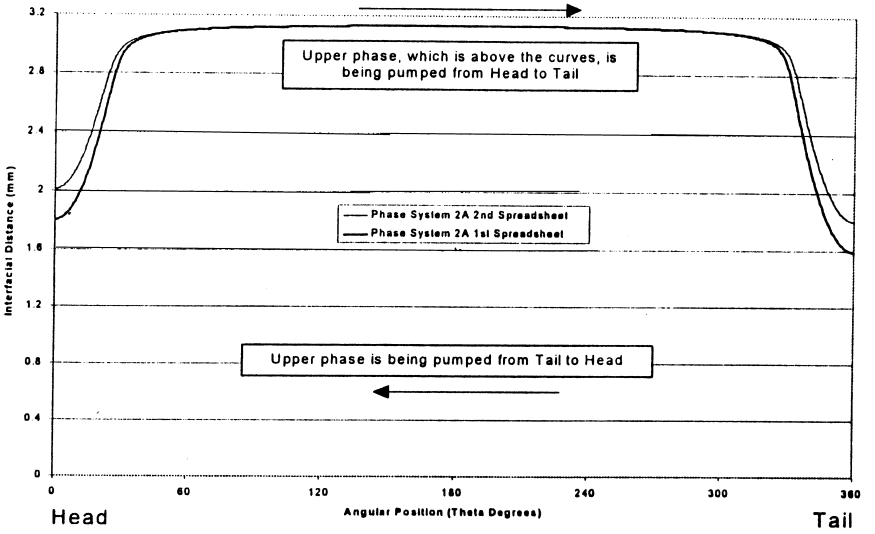

Figure 8. Radial position of the interface for the first and second spreadsheets. This models the change in radial position over one revolution of the centrifuge for the n-Heptane/Water (2A) phase system.

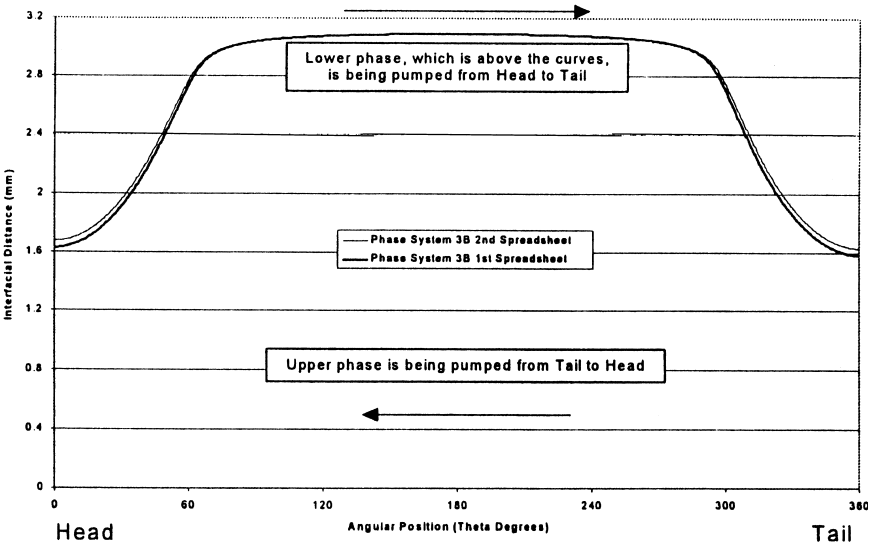

Figure 9. Radial positions of the interface for the first and second calculation mode. This models the change in radial position over one revolution of the centrifuge for the n-Butanol/Water (3B) phase system.

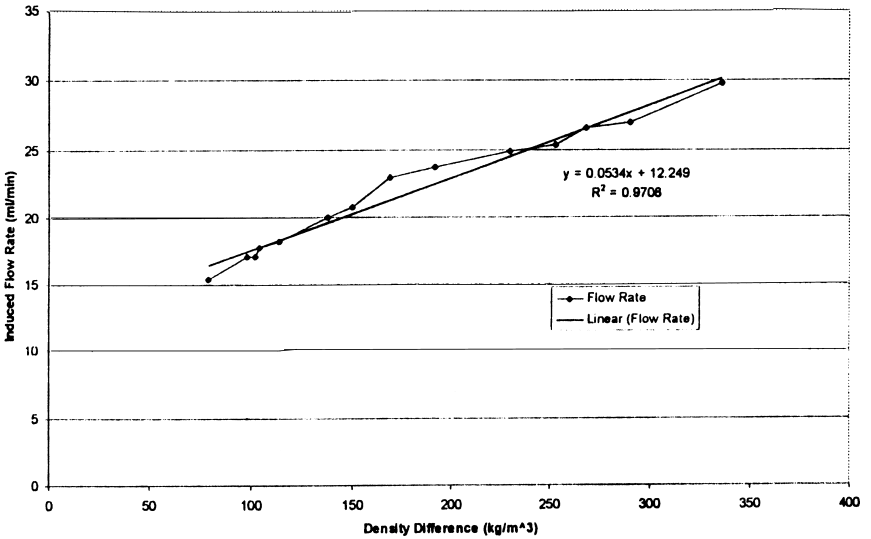

Figure 10. Relationship between density difference and induced flow rate.

4. As θ (angular position) increases, the distance from the head end of the coil is also increasing, hence, the distance to the tail is decreasing. Therefore, the left hand side of a graph can be taken as the head end of the tubing under consideration and the right end as the tail. A change in height of the interface between each end of a graph represents the relative movement (pumping) of the phases through the loop of tubing under consideration.

5. For each curve on figures 6 and 7 there are up to 1440 data points; for reasons of clarity only 21 data points per curve have been plotted. However, the start and end points of each curve are plotted.

DISCUSSION

Comparing phase distribution diagrams for helical coils with a β-value of 0.75 from figure 3 from Ref. [3], with the phase distribution diagrams for spiral coils with 1.6mm bore tubing of figure 4 from Ref. [3], shows that similar retentions were achieved. These phase distribution diagrams were produced with the following conditions:

1. Equal bore diameters for both types of coil, bore diameter of 1.6mm.
2. Equal rotor radius (R=100mm) for both helical and spiral coils.

Table 3. Upper Phase Retention for Two Different Calculations and the Induced Flow Rate of Each Phase

Phase System	Density Diff. Kg/m^3	Upper Phase Ret. % 1st Calculation	Upper Phase Ret. % 2nd Calculation	Change in Upper Phase Retention % 2nd Minus 1st	Induced Flow Rate mL/min
2A	336	94.58	95.81	1.21	29.8
3A	290	93.75	94.85	1.10	26.9
4A	268	93.56	94.64	1.08	26.5
4E	253	93.10	94.14	1.03	25.3
4B	230	92.90	93.91	1.01	24.9
4G	192	92.38	93.35	0.97	23.7
4D	169	92.00	92.94	0.94	23.0
2C	150	90.83	91.68	0.84	20.7
4F	138	90.55	91.37	0.82	20.0
4H	114	89.56	90.30	0.75	18.3
2B	104	88.97	89.69	0.72	17.7
3C	102	88.72	89.42	0.70	17.1
4C	98	88.77	89.47	0.70	17.0
3B	79	87.41	88.04	0.63	15.4

3. Both types of coil were operated over the same speed range, 0 to 1000rpm.

4. β-value range of the spiral coil was 0.5 to 0.8 and the β-value of the helical coil was 0.75.

5. The elution modes (direction of pumping the selected mobile phase) are identical to those recommended in Ref. [1].

Hence, the retention characteristics of spiral and helical coils are similar, providing that the following conditions are met:

1. Similar rotor radius (R) for both helical and spiral coils.
2. Equal bore diameters for both types of coil.
3. Both types of coil are operated at the same speed.
4. Ensure that both types of coil are operated at the same temperature.
5. Ensure that the minimum β-value of the spiral coil is above 0.25.
6. Ensure that the β-value of the helical coil is equal to or greater than the mean of the β-value range of the spiral coil.
7. The spiral coil is rotated in a direction to ensure that the coil is configured head-centre, tail-periphery.
8. The direction of pumping the selected mobile phase (Elution mode) is identical for both types of coil.

9. When the lower phase is selected as the mobile phase, ensure that it is pumped from the head to the tail in both types of coil.

10. When the upper phase is selected as the mobile phase, ensure that it is pumped from the tail to the head in both types of coil.

If the above conditions are met, it is possible to use the retention characteristics obtained in one type of coil to predict the retention characteristics obtained in the other type of coil.

The single layer spiral coil used in Ref. [1] was wound from tubing with an outside diameter of 4.7625mm (3/16") and a bore diameter of 3.175mm (1/8"); the β-value range was 0.38 to 0.85, the rotor radius was 100mm, the rotational speed was 800rpm, the tail end of the coil was at the periphery, and the tests were conducted at 30°C.

The main conclusion of Ref. [1] was that the lower, heavier, phase is always pumped to the tail end of a spiral coil if the tail is placed the at the periphery. Figures 6 and 7 clearly show that there is more lower phase at the tail end of the loop than at the head, indicating that the lower phase is being pumped to the tail replicating the results of Ref. [1]. Figures 8 and 9 compare the position of the interface between the first spreadsheet and the second spreadsheet that is modeled at one revolution later. These figures clearly show that the proportions of upper and lower phases are changing and, hence, pumping is occurring.

Figure 10 shows that the amount of pumping induced in each phase system is proportional to the density difference between the upper and lower phase of each phase system. The linear relationship fitted to the plotted points has a least squares regression coefficient of 0.9708. The scatter of points on either side of the linear relationship is probably due to second order effects, such as the viscosity's of the phases and the interfacial tension. The induced flow rate is, therefore, proportional to the density difference between the phases, however, the relationship does not pass through the origin.

The flow rates shown in table 3 and figure 10 are between 15.4 and 29.8 mL/min and appear to be of the correct magnitude, given that inferred flow rates of between 6 and 30 mL/min were obtained with the spiral coil used in Ref. [1]. When an externally pumped mobile phase is incorporated into the theory, it will be possible to modal the retention characteristics of a phase system given the geometric parameters of a coil and planet centrifuge and the operating conditions.

Equations 37, 40, 41, 44, 48, 49, and 50 bring together the parameters of the J-type centrifuge, the coil geometry, the speed and direction of rotation, and the physical properties of the phase system. The only parameter not used is the interfacial tension of the phase system. Fedotov et al. used interfacial tension and the other parameters to determine the retention of the stationary phase.[4]

In Ref. [4], Fedotov et al. balanced the interfacial tension forces of hydrophobic phase systems with the Archimedean forces generated in a rotating

coil. This retention theory is based upon Archimedean forces breaking the stationary phase up into discrete elements. The retentions predicted by this theory were well matched by experimental results for the following conditions: rotational speeds up to 500rpm, a β-value of 0.37, a flow rate of 1 mL/min; the rotor radius was not listed. There are two hypotheses, Fedotov et al. and the one presented in this paper of how the stationary phase is retained, that have been derived by different methods and result in different equations. However, both hypotheses have shown good correlation to experimental results. The Fedotov et al. hypotheses should be applied when interfacial tension force is significant at low β-values and low rotational speeds and when the stationary phase is likely to be broken into discrete elements. The hypotheses presented in the paper should be used at high β-values and high rotational speeds, when the stationary and mobile phases form continuous stratified layers in the coil, as observed by Conway.[5]

There are combinations of parameters that fall between the categories of low β-values, low rotational speeds and high β-values, high rotational speeds when neither hypothesis can accurately predict the retention. Fedotov and Thiebaut[6] performed retention experiments that may have fallen into this the gap between these categories, while Berthod and Schmitt[7] performed experiments that can be categorized as being high β-value, high rotational speed. Fedotov and Thiebaut did not find a linear relationship stationary phase retention and density difference, however, Berthod and Schmitt did find a linear relationship, see figure 4 Ref. [6] and figures 1 and 2 in Ref. [7]. Table 4 contains the g-levels at which the Fedotov, Thiebaut, and the Berthod, Schmitt experiments were performed and the table also shows the simulated g-levels of the modeled helical coil in this paper. Examination of the g-levels, shows that Berthod and Schmitt's experiments were performed at higher g-levels than those of Fedotov and Thiebaut. As the rotational speed and, hence, the g-levels increase for the Fedotov and Thiebaut experiments, the curves in figure 4 Ref. [6] straighten; the relationship produced at 700 rpm could be fitted with a linear relationship. If another curve had been produced at a higher speed, a linear relationship may have been plotted. The simulated g-levels used to produce the results in figure 6, 7, 8, and 9 are higher than those used by Berthod and Schmitt, and may explain the high coefficient of linear regression of the fitted linear relation in figure 10.

The linear relationship in figure 10 does not pass through the origin and neither do the linear relationships of figures 1 and 2 of Ref. [7]. A possible cause of this is that there is an induced flow when the density difference is zero. Experimentation is required to verify if an induced flow exists with zero density difference and to perform similar experiments as Ref. [7] at higher g-levels and with larger bore tubing to see if the plotted results will pass through the origin.

The retention theory presented in this paper produces a relatively smooth interface between the phases and does not predict the mixing and settling zones observed by Conway in Ref. [5]. The movement of the interface plus the Kelvin-

Table 4. g-Levels Experienced by the Phase Systems in this Paper and in References 6 and 7

Reference	Tangential Acceleration (g-Level)	Radial Acceleration (g-level) Distal Key Node	Proximal Key Node
This paper	72	248 ($\beta = 0.615$)	104 ($\beta = 0.615$)
R = 100mm, 800rpm			
Berthod & Schmitt [7]	43	172 ($\beta = 0.75$)	86 ($\beta = 0.75$)
R = 60mm, 800rpm		107 ($\beta = 0.37$)	21 ($\beta = 0.37$)
Fedotov & Thiebaut [6]	35	108 ($\beta = 0.53$)	39 ($\beta = 0.53$)
R = 63.5mm, 700rpm		88 ($\beta = 0.38$)	18 ($\beta = 0.38$)
Fedotov & Thiebaut [6]	25	80 ($\beta = 0.53$)	29 ($\beta = 0.53$)
R = 63.5mm, 600rpm		64 ($\beta = 0.38$)	13 ($\beta = 0.38$)
Fedotov & Thiebaut [6]	22	67 ($\beta = 0.53$)	24 ($\beta = 0.53$)
R = 63.5mm, 550rpm		54 ($\beta = 0.38$)	11 ($\beta = 0.38$)

The magnitudes of the accelerations were calculated using equations 7 and 8 and dividing by the acceleration due to gravity i.e. 9.81m/s^2.

Helmholtz wave stability criterion are responsible for the zones of mixing and settling and is presented in Ref. [8].

CONCLUSION

The review of Ref. [3] showed that the hydrodynamics of spiral and helical coils are similar, providing that certain experimental conditions are met. The results shown in figures 6, 7, 8, and 9 agree with the results of Ref. [1] when the spiral coil was configured head-centre, tail-periphery. The basic modeling of how the lower phase is pumped to the tail and the upper phase to the head, has been achieved for the condition when the upper and lower phases form continuous stratified layers, as observed in Ref. [5]. This modeling has been achieved for helical coils and needs to be extended for spiral coils.

The equations used to model the hydrodynamic distribution of the phases do not include the interfacial tension. Fedotov et al.[4] produced a mechanism for stationary phase retention that includes interfacial tension. Although, both approaches agree with experimental results and are applicable to certain experimental conditions, knowledge of when to apply the correct model would be useful. There are sets of experimental parameters when neither model provides

accurate results; the inaccuracy is due to the experimental parameters being in the region where the hydrodynamics switches from one model to the other. This is similar to the transition from laminar to turbulent fluid flow and the Reynold's number is used to determine whether laminar or turbulent flow equations should be used. The Reynolds number is a dimensionless group of the flow parameters. A dimensionless group of experimental parameters will hopefully indicate which model to use, and if the prediction will be accurate. Further theoretical and experimental work is required to find such a dimensionless group.

ACKNOWLEDGMENTS

We are grateful for the help of David Hawes and Justin Halls with using the Solver routine from Microsoft Excel, and the writing of macros for Excel.

REFERENCES

1. Sutherland I.A.; Muytjens J.; Prins, M.; Wood, P. A New Hypothesis on Phase Distribution In Countercurrent Chromatography. J. Liq. Chrom. & Rel. Technol. **2000**, *23* (15), 2259-2276.
2. Ito Y. Speculation on the Mechanism of Unilateral Hydrodynamic Distribution of Two Immiscible Solvent Phases in the Rotating Coil. J. Liq. Chromatog. **1992**, *15* (15& 16), 2639-75.
3. Ito Y. Experimental Observations of the Hydrodynamic Behaviour of Solvent Systems in High-speed Countercurrent Chromatography II. Phase Distribution Diagrams for Helical and Spiral Columns. J. Chromatogr. **1984**, *301*, 387-403.
4. Fedotov P.S.; Kronrod V.A.; Maryutina, T.A.; Spivakov, B.Y. On the Mechanism of Stationary Phase Retention in Rotating Coil Columns. J. Liq. Chrom. & Rel. Technol. **1996**, *19* (20), 3237-3254.
5. Conway W.D. *Countercurrent Chromatography Apparatus, Theory and Applications*; VCH Publishers Ltd: U.K., 1990.
6. Fedotov P.S.; Thiebaut, D. Retention of the Stationary Phase in a Coil Planet Centrifuge: Effects of Interfacial Tension, Density Difference and Viscosities of Liquid Phases. J. Liq. Chrom. & Rel. Technol. **1998**, *21* (1 & 2), 39-51.
7. Berthod A.; Schmitt, N. Water-Organic solvent systems in Countercurrent Chromatography: Liquid Stationary Phase Retention and Solvent Polarity. Talanta **1993**, *15* (10), 1489-1498.

8. Wood, P.L.; Sutherland, I.A. Mixing, Settling and the Movement of the Interface Between the Mobile and Stationary Phases in CCC. J. Liq. Chrom. & Rel. Technol. **2000**, submitted for publication.
9. Prins, M. *Countercurrent Chromatography, Research on the Physical Properties*; Brunel University: 1998.

Received September 10, 2000 Author's Revision October 23, 2000
Accepted November 12, 2000 Manuscript 5477